The holocephalan ratfish endoskeleton shares trabecular and areolar mineralization patterns, but not tesserae, with elasmobranchs little skate and catshark

Oghenevwogaga J. Atake[1], Fidji Berio[2], Melanie Debiais-Thibaud[2], B. Frank Eames[1]

[1]Department of Anatomy, Physiology, and Pharmacology, University of Saskatchewan, Saskatoon, Canada

[2] Institut des Sciences de l'Evolution, University of Montpellier, CNRS, IRD, EPHE, Montpellier, France

Correspondence

B. F. Eames,

2D01-107 Wiggins Rd, Saskatoon, SK, S7N 5E5 Canada

Tel: +1 (306)966-6534

Email: b.frank@usask.ca

Website: https://www.eameslab.ca/

Abstract

Specific character traits of mineralized endoskeletal tissues need to be clearly defined and comprehensively examined among extant chondrichthyans (elasmobranchs, such as sharks and skates, and holocephalans, such as chimaeras) to understand their evolution. For example, tiles of mineralized polygonal structures called tesserae occur at cartilage surfaces in chondrichthyans, but recent studies showing trabecular mineralization at elasmobranch cartilage surfaces suggest that tesserae are not as common as previously thought. Also, while areolar mineralized tissue in elasmobranchs is generally considered a unique, shared chondrichthyan feature, some chondrichthyan species demonstrate bone-like tissues in both a specific region of tesserae termed the cap zone and continuous (not tiled) mineralized neural arches. To clarify the distribution of specific endoskeletal features among extant chondrichthyans, adult skeletal tissues in a holocephalan chimaera (spotted ratfish) and two elasmobranchs (small-spotted catshark and little skate) were characterized using synchrotron radiation and desktop micro-CT imaging, and histological and immunofluorescent assays. Endoskeletal mineralization in the ratfish, catshark, and little skate varied both quantitively in tissue mineral density (TMD), and qualitatively in the morphology and localization of mineralized structures and tissues. For example, TMD of several skeletal elements was significantly lower in ratfish, compared to catshark and little skate. Trabecular and areolar mineralization were shared among these extant chondrichthyan species, but tesserae and bone-like tissues were not. Interestingly, three separate analyses argued that the adult chimaera endoskeleton has features of the embryonic little skate endoskeleton. Generally, this

study proposes specific terminology for character states of the extant chondrichthyan endoskeleton and infers those states in ancestral chondrichthyans with reference to fossil data.

Key words: chondrichthyan endoskeleton, mineralization patterns, sharks, skates, chimaeras, tesserae, trabecular, areolar, bone-like tissues, paedomorphism

Introduction

The skeleton of chondrichthyans, or cartilaginous fishes, has long fascinated evolutionary biologists (Daniel, 1934; Janvier, 1996; Kölliker, 1860; Maisey, 2013; Ørvig, 1951; Smith and Hall, 1990; Wurmbach, 1932). However, only in the past two decades has an active research community revealed the histological and molecular complexity of extant chondrichthyan skeletal tissues. Even so, these studies are limited in scope, focussing mostly on specific skeletal features of the Elasmobranchii subclass of extant Chondrichthyes, such as sharks, skates, and rays (Atake et al., 2019; Dean et al., 2017; Eames et al., 2007; Johanson et al., 2012; Kemp and Westrin, 1979; Omelon et al., 2014; Porter et al., 2006; Seidel et al., 2016), with only a few including the Holocephali subclass, such as chimaera (Gillis et al., 2011; Herbert et al., 2022; Pears et al., 2020; Seidel et al., 2020; Smith et al., 2020). Unfortunately, an in-depth description of the extant holocephalan endoskeleton is lacking, leading to a deficit in understanding skeletal tissue character states across extant chondrichthyans.

Like most vertebrates, skeletal mineralization in extant chondrichthyans occurs by incorporation of biominerals into extracellular compartments of skeletal tissues (Golub, 2009; Lowenstam, 1981; Omelon et al., 2014), giving rise to diverse mineralized tissue types in several anatomical sites of the chondrichthyan endoskeleton (Table 1). Traditionally recognized as a defining endoskeletal feature of Chondrichthyes, tesserae form a mineralization pattern consisting of an array of distinct, polygonal units at the surface of cartilages (Kemp and Westrin, 1979; Maisey, 2013; Maisey et al., 2021). In skates, however, a recently characterized trabecular mineralization pattern lies directly underneath the polygonal pattern of tesserae (Atake et al., 2019). In fact, the cartilage surface in several endoskeletal regions of skates and

rays only contains the trabecular mineralization pattern (Atake et al., 2019; Jayasankar et al., 2020), suggesting that polygonal tesserae may not be as common as traditionally thought. Like polygonal tesserae, the little skate trabecular mineralization also forms an arrayed pattern, but the repeating units are in the form of trabecular struts interspersed by unmineralized regions, leading us to call them trabecular tesserae (Atake et al., 2019; Atake and Eames, 2021). Descriptions of a trabecular mineralization pattern in the endoskeleton of sharks or chimaeras are currently lacking, leaving open the possibility that this is a phenotype specific to the Batoidea superorder (including skates and rays) of the subclass Elasmobranchii. In some chimaeras, the surfaces of cartilage in the anterior fused vertebrae (synarcual) and chondrocranium have sheets of mineralization that abut one another (Pears et al., 2020; Seidel et al., 2020), but these do not have an arrayed pattern of repeating units, so perhaps they should not be called tesserae.

Recent evidence suggests that histological features of tesserae may vary according to the mineralization pattern. Traditional polygonal tesserae have distinct histological zones, with a cap zone superficial to a body zone near the surface of chondrichthyan cartilage (Atake et al., 2019; Berio et al., 2021; Kemp and Westrin, 1979; Seidel et al., 2016). While skates have polygonal tesserae, trabecular tesserae in little skate have very small or even absent cap zones overlying extensive body zones (Atake et al., 2019). Additionally, specific regions of tesserae termed spokes are hypermineralized and often devoid of cells, and spokes appear to be a common feature of tesserae regardless of their mineralization pattern (Atake et al., 2019; Pears et al., 2020; Seidel et al., 2020; Seidel et al., 2016). Careful 3D spatial analyses are needed to correlate histological zones and mineralization patterns of tesserae.

91 Some chondrichthyans have mineralized endoskeletal tissues that have been
92 characterized as bone-like (Atake and Eames, 2021). For example, the cap zone of tesserae
93 displays bony features, like elongate cell lacunae in a mineralized ECM of densely packed type I
94 collagen (Col1) fibers (Atake et al., 2019; Kemp and Westrin, 1979; Seidel et al., 2017; Seidel et
95 al., 2016). Unlike the cap zone, the body zone displays typical features of hyaline cartilage,
96 which is the main cartilage type in vertebrates (Goldring et al., 2006). The body zone consists of
97 round chondrocyte lacunae embedded in a mineralized matrix abundant in loosely packed type
98 II collagen (Col2) fibers and sulfated glycosaminoglycans (Enault et al., 2015; Seidel et al., 2017).
99 As another example of bone-like tissue, several elasmobranch species have a non-tiled,
100 mineralized perichondral tissue in their neural arches (Atake et al., 2019; Berio et al., 2021;
101 Bordat, 1987; Eames et al., 2007; Kemp and Westrin, 1979; Seidel et al., 2016). The neural arch
102 bone-like tissue demonstrates morphological and histological features of perichondral bone,
103 including a compact mineralization pattern, elongate cell lacunae, canaliculi-like channels
104 connecting adjacent lacunae, and tightly packed Col1 fibers (Bordat, 1987; Eames et al., 2007;
105 Kemp and Westrin, 1979; Peignoux-Deville et al., 1982; Rossert and de Crombrugghe, 2002;
106 Seidel et al., 2017). Bone-like tissues might be a defining feature of extant chondrichthyans, but
107 relevant data from chimaeras are needed.

108 Finally, areolar mineralized tissue is generally considered a unique feature of the extant
109 chondrichthyan endoskeleton, characterized mostly in elasmobranchs as large sheets of
110 mineralization in the notochordal sheath of the vertebral body (centrum) (Didier, 1995;
111 Ridewood and MacBride, 1921). Areolar mineralized tissue typically contains concentric
112 lamellae of elongate lacunae in a fibrocartilage-like extracellular matrix and a compact

113 mineralization pattern (Atake et al., 2019; Criswell et al., 2017; Dean and Summers, 2006;
114 Eames et al., 2007). Mineralized centra are not thought to be common in chimaeras, but when
115 present, they can appear as multiple mineralized rings in each vertebral segment, which
116 contrasts with the grossly biconcave morphology of segmented centra in elasmobranchs
117 (Gadow and Abbott, 1895).

118 With hopes of revealing shared and clade-specific features among chondrichthyans,
119 here we clarify many of the unresolved issues highlighted above, proposing specific terminology
120 for character states of the extant chondrichthyan endoskeleton (Table 1). Testing the
121 hypothesis that extant chondrichthyans have homologous histological and morphological traits
122 of endoskeletal mineralized tissues, adult tissues in several endoskeletal regions of the spotted
123 ratfish *Hydrolagus colliei* (chimaera), small-spotted catshark *Scyliorhinus canicula* (shark), and
124 little skate *Leucoraja erinacea* (skate) were characterized using synchrotron radiation and
125 desktop micro-CT imaging, and histological and immunofluorescent assays. Tesseral
126 mineralization, cap zones, and neural arch bone-like tissues were absent in the ratfish, but
127 present in these elasmobranchs. Three separate analyses argued that the endoskeleton of this
128 chimaera displays histological and morphological features of the embryonic little skate
129 endoskeleton. While additional chondrichthyan species can bolster these findings, the data
130 argue that trabecular and areolar mineralization patterns, but not tesserae, are shared among
131 extant chondrichthyans. Considering fossil outgroups, we finish by inferring ancestral and
132 derived character states of the chondrichthyan endoskeleton.

133

134 **Table 1. Character states of the mineralized chondrichthyan endoskeleton.** Traits do not apply

135 to all regions of a given fish's skeleton.

Character	State	Description
mineralization patterns	polygonal tesserae (PT)	array of distinct polygonal units between the perichondrium and trabecular tesserae
	trabecular tesserae (TT)	array of distinct trabecular struts, often with hypermineralized spokes, below the perichondrium
	non-tesseral trabeculae (NTT)	non-arrayed, distinct trabecular struts, often with hypermineralized spokes, below the perichondrium
	areolar (AR)	continuous, compact sheets or rings in the notochordal sheath
	bone-like tissue (BLT)	continuous, compact regions between the perichondrium and a cartilaginous core, often in neural arches and cap zones
histological features	body zone (BZ)	distinct region of mineralized tissue below the perichondrium, containing Col2, rounded cell lacunae, and low-cellularity spokes
	cap zone (CZ)	distinct region of mineralized tissue between the perichondrium and body zone, containing tightly-

		wound Col1 fibers and elongated cell lacunae
	bone-like tissue (BLT)	mineralized tissue of tightly-wound Col1 fibres and elongated cell lacunae connected by canaliculi-like channels

Results

Adult mineralized tissues in spotted ratfish had lower tissue mineral density (TMD) than small-spotted catshark or little skate

To assess whether chimaeras demonstrate skeletal mineralization in anatomical sites that are homologous to those of elasmobranchs, 3D rendering of micro-CT images of anterior regions of adult ratfish were qualitatively and quantitatively analyzed (Fig. 1A,B). Micro-CT images revealed mineralized tissues in several endoskeletal regions, including neural arches and centra of segmented vertebrae (Fig. 1C,D), skeletal elements in the pharyngeal skeleton (Fig. 1E), and the fused vertebral synarcual (Fig. 1F,G). Although elasmobranchs mineralize neural arches in their precaudal and caudal vertebrae (Atake et al., 2019; Berio et al., 2021; Eames et al., 2007), mineralized neural arches were present mainly in precaudal vertebrae of ratfish (Fig. 1C,D; data not shown). Mineralized skeletal elements in the pharyngeal skeleton included the basihyal, Meckel's, ceratohyal, basibranchial, hypobranchials, and ceratobranchial (Fig. 1E). Spinal nerve foramina are common in the synarcual of cartilaginous fishes and were present in the ventral sides of the ratfish synarcual (Fig. 1F; Claeson, 2011; Johanson et al., 2015; Pears et al., 2020). Unlike the synarcual in skates and other batoids, where mineralized centra are not

153 discernible (Atake et al., 2019; Claeson, 2011), the synarcual in ratfish had distinct mineralized
154 centra for its entire length (Fig. 1G).

155 TMDs of the synarcual, neural arches, and centra in ratfish, catshark, and little skate
156 were quantitated and compared, where possible, since sharks do not have a synarcual (Fig. 1H).
157 Because little skate does not have centra within the synarcual, centra in the ratfish synarcual
158 were digitally segmented and excluded for synarcual TMD data. The average TMD of the ratfish
159 synarcual was 0.31± 0.11 gHA/cm^3, significantly lower than the TMD of the little skate
160 synarcual, which was 0.94 ± 0.04 gHA/cm^3 (Fig. 1H; p= 6.5x10^{-4}). Similarly, the TMD of ratfish
161 neural arches (0.40 ± 0.05 gHA/cm^3) was significantly lower than the TMD of neural arches of
162 either catshark (0.81 ± 0.04 gHA/cm^3; p=9 x10^{-6}) or little skate (0.96 ± 0.04 gHA/cm^3; p=4.5x10^{-7};
163 Fig. 1H). The average TMD of ratfish centra (0.42 ± 0.10 gHA/cm^3) was also significantly lower
164 than the TMD of centra of either catshark (0.84 ± 0.02 gHA/cm^3; p=1.1 x10^{-4}) or little skate (0.88
165 ± 0.05 gHA/cm^3; p=3.4 x10^{-5}; Fig. 1H). In ratfish, TMD of segmented centra within the synarcual
166 was similar to that of centra in segmented vertebrae (0.46 ± 0.11 gHA/cm^3). These analyses
167 showed that the synarcual, neural arches, and centra in ratfish had significantly lower TMDs
168 compared to homologous elements in catshark and little skate.

169

170 **Neural arches in ratfish lacked bone-like tissue**

171 To clarify whether chimaeras have bone-like tissue like elasmobranchs, micro-CT and
172 histological analyses of neural arches in segmented precaudal vertebrae of ratfish were
173 compared to neural arches in segmented precaudal vertebrae of catshark and little skate.
174 Mineralization of neural arches in ratfish was organized in a non-continuous pattern of small

175 compact and trabecular regions (Fig. 2A). This mineralization pattern in spotted ratfish
176 contrasted with the continuous mineralization pattern displayed by the compact, bone-like
177 tissue in catshark and little skate (Fig. 2B,C; Atake et al., 2019; Berio et al., 2021). Furthermore,
178 cross-section views demonstrated that mineralized tissues in ratfish were restricted to the
179 medial and lateral periphery of the neural arches (Fig. 2D). By contrast, mineralization of bone-
180 like tissues in catshark and little skate extended much deeper in the neural arch (Fig. 2E,F).

181 Histologically, Alizarin red staining of calcium showed that mineralized tissues in ratfish
182 neural arches were much thinner and not continuous like bone-like tissues in catshark and little
183 skate neural arches (Fig. 2G-I). Alcian blue staining of sulfated proteoglycans marked cartilage in
184 most neural arch regions in ratfish, while only the cartilaginous core regions of catshark and
185 little skate neural arches were Alcian blue-positive (Fig. 2G-I). The neural arch core in catshark
186 was mostly unmineralized cartilage, while that of little skate was mineralized cartilage (Fig.
187 2H,I). Birefringence of picrosirius-stained, tightly packed collagen fibers (likely reticular) were
188 observed in muscles lateral to neural arches in all three species (Fig. 2J-L). Birefringence was not
189 observed in ratfish neural arches, whereas birefringence in neural arch bone-like tissues was
190 observed in catshark and little skate (Fig. 2K,L). Most regions (including unmineralized cartilage
191 and mineralized tissue) in ratfish neural arches demonstrated Col2 immunofluorescence (Fig.
192 2J). Only the cartilaginous core in neural arches of catshark and little skate demonstrated Col2
193 immunofluorescence (Fig. 2K,L). These results showed that bone-like tissue was absent in
194 neural arches of ratfish, and the non-continuous pattern of mineralized tissue in ratfish neural
195 arches was mineralized cartilage.

196

197 **Novel characterization of non-tesseral trabecular mineralization in ratfish and catshark**
198 **showed the absence of a bone-like cap zone**

199 To clarify whether tesserae are defining endoskeletal features of extant
200 chondrichthyans, morphological patterns and histological features of mineralized tissues were
201 characterized in ceratohyals of ratfish, caudal vertebrae of catshark, and precaudal vertebrae
202 and hyomandibulae of little skate. Desktop micro-CT renderings of ratfish ceratohyals and
203 catshark haemal arches revealed mineralized tissues with a trabecular pattern like that of
204 trabecular tesserae in the vertebral neural spine of little skate (Fig. 3A-G). However, the
205 trabecular pattern in ratfish and catshark was not as clearly organized into arrays of repeating
206 trabecular units like that of trabecular tesserae in little skate, and for this reason, trabecular
207 patterns in ratfish and catshark were characterized as non-tesseral. In the hyomandibulae and
208 other skeletal elements of little skate, including synarcual, propterygium, and vertebral
209 transverse processes, a trabecular mineralization pattern occurred underneath the superficial
210 polygonal tesseral pattern (Fig. 3D,H,H'; Atake et al., 2019). Notably, many regions in ratfish
211 (vertebrae, pharyngeal skeleton, and the synarcual) and catshark (vertebrae and ceratohyals)
212 did not exhibit the polygonal mineralization pattern typical of tesserae (Atake et al., 2019;
213 Kemp and Westrin, 1979; Maisey, 2013; Marramà et al., 2019; Seidel et al., 2016; Wilga and
214 Ferry, 2015).

215 To assess whether trabecular mineralized tissues in ratfish, catshark, and little skate
216 exhibit similar histological features, cross sections of tissues with non-tesseral patterns were
217 compared to those with tesseral patterns. Non-tesseral mineralized tissues in Alcian blue-
218 positive perichondral regions in ratfish ceratohyals and catshark haemal arches stained with

219 Alizarin red (Fig. 3I,J; perichondrium marked by straight dashed line). The discrete organization
220 of mineralized tissues and Alcian blue and Alizarin red staining patterns of non-tesseral
221 mineralized tissues in ratfish and catshark were similar to the tesseral body zone in little skate
222 (Fig. 3I-L). However, Alcian blue-positive cartilage separated Alizarin red-positive non-tesseral
223 mineralized tissues from overlying perichondrium in ratfish and catshark (Fig. 3I,J). A bone-like
224 cap zone just below the perichondrium was only present in tesseral mineralized tissues in little
225 skate (Fig. 3K,L; perichondrium marked by straight dashed line). The bone-like cap zone stained
226 more intensely than the body zone with Alizarin red and was relatively smaller and larger in
227 trabecular tesserae and polygonal tesserae, respectively (Fig. 3K,L). Perichondrium of both non-
228 tesseral and tesseral mineralized tissues stained with the general connective tissue dye fast
229 green (Fig. 3M-P). Matrix of the little skate bone-like cap zone was fast green-positive and had
230 birefringent collagen fibers, but these staining patterns were not observed in non-tesseral
231 mineralized tissues in ratfish and catshark (Fig. 3M-T). Instead, regions just below the
232 perichondrium of ratfish ceratohyals and catshark haemal arches stained for sulfated
233 proteoglycans by Safranin O and were Col2-positive cartilage (Fig. 3M,N,Q,R). Staining patterns
234 of non-tesseral mineralized tissues in ratfish and catshark were generally consistent with those
235 of mineralized cartilage in the tesseral body zone of little skate, although chondrocyte lacunae
236 in these regions were not obvious in ratfish (Fig. 3I-T). Therefore, histological features of
237 trabecular mineralized tissues in ratfish ceratohyals and catshark haemal arches were similar to
238 only the body zones of tesserae in little skate, which consisted of mineralized cartilage.
239

240 **Spatial organization of histological features correlated with trabecular and polygonal**
241 **mineralization patterns**

242 Given that trabecular mineralized tissues typically have small or even absent cap zones,
243 and polygonal tesserae typically have large cap zones, histology and micro-CT segmentation
244 were used to see whether there was a correlation between histological features and
245 mineralization patterns in ratfish and little skate. After demineralization, non-tesseral tissues in
246 ratfish and tesseral tissues in little skate exhibited spokes, which are regions of very low
247 cellularity in the body zone that often appeared as tears or sectioning artifacts and did not stain
248 strongly with any Trichrome dye (Fig. 4A-C). Non-spoke regions of the body zone stained either
249 slightly blue for collagen fibers with Trichrome's aniline blue or magenta with Trichrome's acid
250 fuchsin, and these staining patterns were consistent in non-tesseral and tesseral tissues.
251 Tightly-wound collagen fibers were marked by Trichrome's acid fuchsin, but only in the larger
252 and smaller cap zones of little skate polygonal and trabecular tesserae, respectively (Fig. 4A-C).
253 Also, the presence of elongate lacunae distinguished the cap zone from other tesseral regions
254 (Fig. 4A-C).

255 Enough histological features were also visible in synchrotron radiation micro-CT
256 renderings (Fig. 4D-F), making it possible to segment and analyze the spatial correlation
257 between mineralization patterns and histological features, such as cap zone and spokes (red
258 and blue, respectively, in Fig. 4G-I). Segmentation of 3D renderings of deep surface views
259 showed that hypermineralized spokes were localized to non-tesseral and tesseral trabecular
260 mineralization patterns in ratfish and little skate, respectively (blue in Fig. 4J-L). Unlike the well-
261 organized spokes seen in trabecular patterns of little skate tesserae, spokes in ratfish trabecular

262 mineralized tissues were patchy and less-organized. Therefore, both non-tesseral and tesseral
263 trabecular mineralization patterns correlated with, and appeared to derive from, spokes and
264 non-spoke regions within body zones.

265 Unlike little skate polygonal tesserae, trabecular mineralized tissues in ratfish and
266 trabecular tesserae in skate both displayed identical trabecular mineralization patterns whether
267 viewed from the superficial or deep surfaces of the cartilage (Fig. 4J,K,M,N). The smaller cap
268 zones in trabecular tesserae were discernible on the superficial surface, but they were not as
269 laterally extensive as cap zones of polygonal tesserae (Fig. 4H,I,N,O). Thus, larger and laterally
270 extensive cap zones appeared to be the reason why polygonal tesserae displayed a superficial
271 polygonal mineralization pattern.

272

273 **Ratfish centra contained areolar mineralized tissue**

274 To clarify whether ratfish, catshark, and little skate have areolar mineralized tissue,
275 morphological and histological features of centra were revealed by desktop micro-CT and
276 section histology. Precaudal vertebrae in ratfish had multiple rings of centra per vertebral
277 segment (i.e., unit with paired neural arches and basidorsals; Fig. 5A). Each centrum in ratfish
278 precaudal vertebrae demonstrated a compact mineralization pattern like that of centra in the
279 catshark and little skate (Fig. 5A-C). However, no ratfish centrum displayed the typical
280 biconcave gross morphology associated with elasmobranch centra (Fig. 5A-C; (Atake et al.,
281 2019; Clement, 1992; Criswell et al., 2017).

282 Alizarin red and Alcian blue section histology showed that centra in ratfish, catshark,
283 and little skate comprised of compact mineralized tissue spanning different numbers of

284 centrum layers. The ratfish centrum only had mineralized tissue in the middle layer, but an
285 outer layer of the catshark centrum had mineralized cartilage, while inner and outer layers of
286 the little skate centrum contained mineralized cartilage (Fig. 5D-I). Areolar mineralized tissues
287 in the middle layer of the centrum of ratfish, catshark, and little skate had elongate cell lacunae
288 organized in concentric lamellae (inserts in Fig. 5G-I; Atake et al., 2019; Criswell et al., 2017;
289 Eames et al., 2007), and they were birefringent (data not shown). Markers of cartilage differed
290 in areolar mineralized tissue among ratfish, catshark, and little skate (Fig. 5J-O). In ratfish,
291 areolar mineralized tissue had relatively strong Safranin O staining and Col2
292 immunofluorescence (Fig. 5J,M). Areolar mineralized tissue in catshark demonstrated weak
293 Safranin O staining and Col2 immunofluorescence (Fig. 5K,N). By contrast, areolar mineralized
294 tissue in little skate did not display Safranin O staining or Col2 immunofluorescence (Fig. 5L,O).
295 Overall, these data suggested that ratfish have areolar mineralized tissue.
296
297 **Qualitative and quantitative features of centra in the adult ratfish were similar to those of**
298 **little skate embryos**
299 The biconcave centra morphology is thought to be acquired in elasmobranchs during
300 development when the perichordal sheath becomes constricted by mesenchymal cells (Arratia
301 et al., 2001; Gadow and Abbott, 1895; Kölliker, 1860). To shed light on differences in adult
302 centra morphology, morphological and histological features of centra in a developmental series
303 of little skate were compared to those of adult ratfish. In little skate embryos and hatched
304 juveniles, desktop micro-CT renderings showed mineralization in the centrum and pairs of
305 neural arches, basidorsals, and haemal arches of each vertebral segment (Fig. 6A-C). Expanding

306 upon recent work showing that anterior and posterior segments of somites fuse during skate
307 vertebral development, similar to tetrapods (Criswell and Gillis, 2020), independent anterior
308 and posterior mineralizations of each interneural appeared to later fuse during development.
309 For example, independent mineralization of the posterior and anterior interneurals were visible
310 in stage 32 little skate embryos, whereas the dorsal and ventral aspects of each appeared fused
311 by stage 33, and they were fully fused in a 6.5cm DW juvenile (Fig. 6A-C). In adult ratfish, each
312 vertebral segment of paired neural arches and basidorsals had an average of six centra (Fig.
313 6D). Digital segmentation of synchrotron radiation (SR) micro-CT renderings showed that centra
314 in little skate stage 32 embryos were slightly constricted in the middle of each element's
315 anterior-posterior axis, and the extent of this constriction progressed through 6.5 cm disc width
316 (DW) juveniles, when the classic biconcave morphology was present (Fig. 6E-G). SR micro-CT
317 renderings showed that adult ratfish centra were constricted to a similar extent as younger
318 centra in little skate embryos (Fig. 6E,F,H). In little skate embryos, Alcian blue and Alizarin red
319 section histology showed that the areolar mineralized tissue initiated in the middle layer of the
320 centrum and had elongate cell lacunae organized in concentric lamellae, similar to that
321 observed in adult ratfish (Fig. 5D; Fig. 6I,J). At later developmental stages of little skate, such as
322 6.5 cm DW juveniles, the outer layer of the centrum also demonstrated mineralized cartilage
323 (Fig. 6K).

324 To further confirm these morphological and histological similarities of centra in little
325 skate embryos and adult ratfish, TMDs of centra in the developmental series of little skate were
326 compared to that of adult ratfish. TMD of little skate centra increased significantly from stage
327 32 to stage 33 embryos (p= 9.5 x10^{-3}), while TMD of 6.5 cm DW juveniles was only significantly

328 higher than TMD of stage 32 embryos (Fig. 6L; p=9.6 x10^{-4}). TMD of adult ratfish centra was
329 significantly higher than TMD of centra in little skate stage 32 embryos, but it was statistically
330 indistinguishable from TMD of centra in little skate stage 33 embryos and 6.5 cm DW juveniles
331 (Fig. 6L). Therefore, adult ratfish centra had morphological, histological, and TMD similarities
332 with centra from little skate embryos, particularly those at stage 33.
333

334 **Discussion**

335 Which tissues are common in the extant chondrichthyan endoskeleton? Bone-like and
336 areolar tissues have been characterized in several members of the chondrichthyan subclass
337 Elasmobranchii, such as sharks, skates, and rays (Atake et al., 2019; Berio et al., 2021; Bordat,
338 1987; Kemp and Westrin, 1979; Ørvig, 1951; Peignoux-Deville et al., 1982; Seidel et al., 2016). In
339 addition, polygonal tesserae are traditionally associated with chondrichthyans (Atake et al.,
340 2019; Kemp and Westrin, 1979; Maisey, 2013; Marramà et al., 2019; Seidel et al., 2016; Wilga
341 and Ferry, 2015), but trabecular tesserae were recently characterized in skates and rays (Atake
342 et al., 2019; Jayasankar et al., 2020).

343 Two main qualities of this paper go a long way in revealing features of the ancestral
344 chondrichthyan endoskeleton. First, we explicitly identifed discrete character states of extant
345 chondrichthyan endoskeletons (Table 1), helping to unify terminology of important features for
346 the growing chondrichthyan research community. Second, we presented extensive, side-by-side
347 comparative data across various extant chondrichthyans, two elasmobranch species (small-
348 spotted catshark and little skate) and one chimaera/holocephalan (spotted ratfish). Including
349 ratfish is another critical aspect of this paper, because holocephalans are generally

350 understudied, but must be considered when inferring ancestral chondrichthyan traits.
351 Importantly, previous characterization of skeletal mineralization in other adult chimaeridae
352 neither focused on segmented neural arches to analyze bone-like tissues or areolar
353 mineralization, nor clarified histological zones of tesserae (Berio et al., 2021; Debiais-Thibaud,
354 2018; Pears et al., 2020; Seidel et al., 2020)

355 Our new data and other published data across various extant and fossil chondrichthyan
356 species can be compiled to compare character states of the extant endoskeleton and infer the
357 ancestral condition (Fig. 7). In what appears to be a novel character trait of crown
358 chondrichthyans, trabecular mineralization occurs in many endoskeletal regions in several
359 elasmobranch and chimaera species, including some fossil chondrichthyans (Atake et al., 2019;
360 Coates et al., 2018; Jayasankar et al., 2020; Maisey et al., 2021; Ørvig, 1951). Among extant
361 chondrichthyans, trabecular mineralization always forms near the surface of cartilage, but the
362 exact mineralization pattern varies. Little skate, along with all other batoids and some
363 selachians examined, have arrayed patterns of discrete trabecular units, similar to the
364 repeating polygonal units of traditional tesserae, supporting their description as trabecular
365 tesserae. On the other hand, a non-arrayed trabecular mineralization pattern, not emphasized
366 in chondrichthyans before, appears to be present in catshark and some other selachians and in
367 ratfish and all other chimaeras examined, including *Callorhinchus milii* and *Chimaera monstrosa*
368 (Pears et al., 2020; Seidel et al., 2020). To distinguish this pattern from the regular, arrayed
369 patterns of polygonal and trabecular tesserae, we propose the term "non-tesseral trabecular
370 mineralization". Given that some fossil chondrichthyans, such as *Gladbachus*, *Climatius*,
371 *Doliodus,* and *Cobelodus*, also appear to display this mineralization pattern in their

372 endoskeletons (Coates et al., 2018; Maisey et al., 2021; Ørvig, 1951), non-tesseral trabecular
373 mineralization might be a new plesiomorphic (ancestral) character of chondrichthyans (Maisey
374 et al., 2021).

375 Bone-like tissues do not appear to be shared among extant chondrichthyans, while
376 areolar mineralization does seem to be shared (Fig. 7). Morphological and histological features
377 of bone-like tissues in neural arches or tesseral cap zones are present in catshark, little skate,
378 and many other elasmobranch species, but absent in ratfish and *C. monstrosa* (Atake et al.,
379 2019; Berio et al., 2021; Eames et al., 2007; Kemp and Westrin, 1979; Seidel et al., 2020; Seidel
380 et al., 2017; Seidel et al., 2016; Wurmbach, 1932). While these data refute the hypothesis that
381 bone-like tissues generally are a symplesiomorphic (shared ancestral) feature of extant
382 chondrichthyans, they further support the hypothesis that neural arch perichondral bone-like
383 tissue is a synapomorphic (shared derived) character of elasmobranchs, but subsequently lost
384 in several lineages (Atake et al., 2019; Berio et al., 2021; Maisey et al., 2021). On the other
385 hand, similar features of centra are observed in ratfish, catshark, little skate, and many other
386 extant chondrichthyans examined (Atake et al., 2019; Criswell et al., 2017; Dean and Summers,
387 2006; Debiais-Thibaud, 2019; Eames et al., 2007; Porter et al., 2006). Since most data on areolar
388 mineralization focussed on elasmobranchs (Criswell et al., 2017; Eames et al., 2007; Ridewood
389 and MacBride, 1921), histological features of multiple-ringed centra in other chimaera should
390 be determined (Didier, 1995). Stem chondrichthyans did not appear to mineralize their centra,
391 so data from extant chondrichthyans argue that areolar mineralized tissue is likely a
392 synapomorphic character of crown chondrichthyans (Frey et al., 2019; Maisey et al., 2021;
393 Miles, 1970).

Cap and body zones are histological terms that traditionally describe chondrichthyan tesserae (Dean and Summers, 2006; Kemp and Westrin, 1979), but data from adult samples of ratfish, catshark, little skate, and several other species argue that the body zone is the only histological zone of endoskeletal mineralization shared by extant chondrichthyans (Fig. 7). Recent histological data of tesserae are few and limited to sharks, skates, and rays, where cap and body zones have been reported (Atake et al., 2019; Berio et al., 2021; Eames et al., 2007; Enault et al., 2015; Kemp and Westrin, 1979; Seidel et al., 2017). While birefringent fibers marked the cap zones in both polygonal and trabecular tesserae in little skate, non-tesseral trabeculae in catshark and ratfish did not have discernible cap zones. In contrast to commonly-accepted knowledge, these catshark data suggest that even sharks do not always have the cap zone. Taken alongside recent published data (Maisey et al., 2021; Pears et al., 2020; Seidel et al., 2020), no living species of chimaera likely has cap zones. On the other hand, Safranin O staining and Col2 immunofluorescence showed that histological body zones generated the mineralized endoskeletal cartilage of ratfish, catshark, and little skate. In total, these data suggest that the ancestral stem chondrichthyan generated most of its endoskeletal mineralization with histological body zones, although as the next paragraph highlights, cap zones might have been lost secondarily in chimaera and some shark species.

Digitally segmented 3D regions of micro-CT renderings showed, for the first time, exact spatial correlations between histological zones and mineralization patterns, potentially impacting histological interpretations of fossils. Strikingly, large and laterally extensive cap zones were the basis of the traditional polygonal tesseral mineralization pattern in little skate. Accordingly, similar polygonal tesserae recently described in fossil holocephalans likely have

416 cap zones in addition to body zones and a trabecular tesseral mineralization underlying the
417 polygonal mineralization pattern, and these might have been lost secondarily during
418 holocephalan evolution (Fig. 7; Atake et al., 2019; Pears et al., 2020). Increased descriptive
419 power from synchrotron imaging of polygonal tesserae in fossil elasmobranchs and
420 holocephalans can clarify this point. Two other correlations were identified here in body zones.
421 First, spokes were located in body zones. Second, spoke and non-spoke regions of the body
422 zone comprised the trabecular mineralization patterns, regardless of whether these were
423 organized as arrayed tesserae or not. Spokes appeared much more spatially organized in
424 polygonal tesserae and trabecular tesserae than in the non-tesseral trabecular mineralization
425 pattern. By extension of the body zone correlation with trabecular mineralization, trabecular
426 mineralization of some fossil elasmobranchs and holocephalans like *Palaeobates polaris* and
427 *Cladoselache* might derive solely from body zones (Maisey et al., 2021; Ørvig, 1951). Given such
428 dramatic variation in extant and fossil chondrichthyans, cellular and molecular mechanisms
429 underlying the evolution of tesseral and non-tesseral mineralization patterns is a wide open
430 field of future study.

431 Finally, three independent features suggested that the adult ratfish endoskeleton
432 shared features of the embryonic little skate endoskeleton. First, tissue mineral density (TMD)
433 was significantly lower in a number of adult ratfish endoskeletal elements, compared to adult
434 catshark and little skate. In fact, the TMD of adult ratfish centra was indistinguishable from the
435 TMD of embryonic little skate centra. Second, in contrast to previous assertions that
436 mineralized centra in chimaeras were unconstricted (Didier, 1995; Gadow and Abbott, 1895),
437 micro-CT renderings of ratfish centra showed slight constriction, which was like those of centra

438 in little skate embryos. Third, even histological similarities of centra in little skate embryos and
439 adult ratfish were discovered. Both had elongate cell lacunae organized in concentric lamellae
440 only in the mineralized middle layer of the centrum.

441 A tantalizing possibility is that the similarities between adult ratfish and embryonic little
442 skate endoskeletons represents the effects of a phenomenon termed paedomorphism, or the
443 derived condition of an adult species retaining embryonic traits of an ancestor (Garstang, 1922;
444 Liem, 2001). Given lower TMD in many adult ratfish endoskeletal elements, the ratfish might
445 generally have paedomorphic endoskeletal development, because as mineralized skeletal
446 tissues develop, their TMD tends to increase (Forbes, 1976). The genetic basis for reduced
447 skeletal mineralization in chimaeras should be investigated further, especially since the only
448 published full chondrichthyan genome was from *Callorhinchus milii* (Callorhinchidae)
449 (Venkatesh et al., 2014), and Callorhinchidae is the only chimaera family, for example, that does
450 not mineralize their centra (Fig. 7; Didier, 1995; Gadow and Abbott, 1895). Our findings on
451 slight constriction of centra in both adult ratfish and embryonic little skate independently
452 supported a previous assertion that the perichordal sheath in adult chimaeras remained at a
453 stage corresponding to that of embryonic elasmobranchs (Gadow and Abbott, 1895). Additional
454 future discoveries, however, would be needed to support the idea that the endoskeleton of
455 ratfish (perhaps even extant holocephalans generally) is paedomorphic with respect to that of
456 the common ancestor of holocephalans and elasmobranchs. First, these traits (lower
457 endoskeletal TMD, slight morphological constriction of centra, and elongated lacunae in the
458 only mineralized (middle) layer of centra) must be present in this last common ancestor.

Second, primitive holocephalans must have altered these traits. Hopefully, paleontologists can resolve these issues.

In summary, analyses of extant and fossil data suggest different features of the chondrichthyan endoskeleton appeared (and disappeared) at different times during evolution of this fascinating clade (Fig. 7). The widespread distribution of non-tesseral trabecular mineralization among fossil stem and extant crown chondrichthyans argue that this is a symplesiomorphic chondrichthyan character. Areolar mineralization is widespread among extant chondrichthyan species, but absent in early stem chondrichthyans, suggesting it evolved in a later stem chondrichthyan that gave rise to holocephalans and elasmobranchs. The presence of tesserae in extant elasmobranchs and the fossil holocephalan *Cobelodus* argues that this trait was lost secondarily in extant holocephalans. Bone-like tissues in cap zones or neural arches appears restricted to extant elasmobranchs. Extant species have correlations between the histological body zone and any form of trabecular mineralization on the one hand, and the cap zone and polygonal tesserae on the other. Given these correlations, the body zone might also be symplesiomorphic for all chondrichthyans, while the cap zone might be synapomorphic for crown chondrichthyans, secondarily lost in extant holocephalans.

Materials and Methods

Specimens

All samples were approved for use under the University of Saskatchewan ethical protocol (AUP 20130092). Vertebrae (precaudal and caudal) from three samples of adult small-spotted catshark with total lengths of 31 cm were provided by the University of Montpellier

481 Aquarium (Planet Ocean Montpellier). Adult, juvenile, and embryonic samples of the little skate
482 were obtained from Marine Biological Labs (Falmouth, MA, USA). Four samples of adult little
483 skate with total lengths (TL) ranging from 43.5 cm – 47.5 cm were sampled (SupTable 1). Little
484 skate juveniles (n=7) were staged by measuring their TL and disc widths (DW) and ranged from
485 5.5 cm DW, 10 cm TL to 6.5 cm DW, 11 cm TL (SupTable 1; Stehmann, 2002). The average DW
486 and TL of stage 32 embryos (n=6) and stage 33 embryos (n=6) were 3.2 cm DW, 7.5 cm TL and
487 3.5 cm DW, 8 cm TL, respectively (SupTable 1; Maxwell et al., 2008; Vazquez et al., 2020). Five
488 samples of adult spotted ratfish with total lengths ranging from 28.5 cm to 45 cm were
489 captured by deep-water trawl in the San Juan Islands, WA, frozen within one or two hours of
490 catch, and kept frozen for several years until thawed for experiments (SupTable 1).

491 Regions of interest, such as ceratohyal, synarcual, and precaudal and caudal vertebrae,
492 were dissected from the little skate, catshark, and ratfish samples (SupTable 1). Dissected
493 tissues were preserved by fixation in 4% paraformaldehyde in PBS (pH 7.4) and dehydrated
494 through a graded ethanol series.

495

496 **Micro-CT imaging and data processing**

497 Desktop micro-CT imaging of ratfish ROIs, little skate ROIs, and catshark precaudal
498 vertebrae was done using SkyScan 1172 desktop microtomograph (Bruker SkyScan, Kontich,
499 Belgium). Desktop micro-CT projections were acquired using a 0.5 mm aluminium filter at 40 kV
500 and 250 µA, 100 ms exposure time, and 10 µm voxel resolution, and reconstructed using
501 NRecon (Bruker SkyScan, Kontich, Belgium). A lower resolution projection (i.e., 26 µm voxel,
502 700 ms exposure time) of an anterior region of the ratfish was acquired in parts (Fig. 1A). Scans

503 from the different parts were later stitched together using Dragonfly v2021.1 (Object Research
504 Systems, Canada). Desktop imaging of catshark caudal vertebrae was performed using CT
505 scanner: EasyTom 150 scanner at 70 kV, 80 µA, 1.43 s exposure time, and 6 µm voxel
506 resolution. Reconstructions were done with Xact software (v11025) images were rendered with
507 Avizo Lite software (v2019.3). Tissue mineral density (TMD) of ratfish, little skate, and catshark
508 ROIs was quantitated on SkyScan 1172 desktop micro-CT images using CTAnalyzer v1.16 (CTAn,
509 Bruker SkyScan, Kontich, Belgium) as previously described (Atake et al., 2019).

510 Synchrotron radiation (SR)-based micro-CT imaging of ratfish and little skate was done
511 on the Biomedical Imaging and Therapy-Insertion Device 05ID-2 (BMIT-ID) line at the Canadian
512 Light Source. SR micro-CT projections were acquired with a 28 keV photon energy, 1.44 µm
513 voxel resolution, 1s exposure time, and a sample to detector distance of 9 cm. Reconstruction
514 of SR micro-CT projections and phase retrieval was done using UFO-KIT software
515 (https://github.com/ufo-kit/ufo-core.git). A delta/beta ratio of 200 was applied during phase
516 retrieval. 3D rendered volumes and 2D virtual slices of reconstructed data were generated with
517 Amira 6.0 (FEI Group, USA). 3D segmentation and color-coding of morphological features were
518 done using segmentation editor tools in Amira.

519

520 **Histological and immunofluorescence assays**

521 Tissues for section histology were not demineralized before sectioning. Tissues were
522 embedded in optimum cutting temperature compound (Tissue Tek, Torrance, CA, United
523 States), and serial tissue sections of 10 µm thickness were made with a Cryostar NX50 cryostat
524 (Fisher Scientific, United States).

525 Tissue sections were stained as described with Safranin O (Ferguson et al., 1998),
526 picrosirius red (Junqueira et al., 1978), or Milligan's Trichrome (Ashique et al., 2022). Alcian
527 blue/Alizarin red staining was done using a modified acid-free protocol (Eames et al., 2011).
528 Briefly, tissues sections were washed with 100 mM Tris pH 7.5/10 mM $MgCl_2$, stained with
529 0.04% Alcian blue/70%EtOH/10mM $MgCl_2$ pH 7.5, taken through graded EtOH series (80%
530 EtOH/100 mM Tris pH 7.5/10 mM MgCl2; 50% EtOH/100 mM Tris pH 7.5; 25% EtOH/100 mM
531 Tris pH 7.5), stained with 0.1% Alizarin red/0.1 % KOH pH 7.5, de-stained with two washes of
532 0.1% KOH, and dehydrated through 25% EtOH, 50% EtOH, 80% EtOH, and 100% EtOH series
533 before coverslipping. Tissue sections were demineralized using 5% EDTA for 10 mins before
534 staining with Safranin O to improve staining of mineralized cartilage.

535 To minimize the chances of tissues falling off slides, tissue sections for
536 immunofluorescence were incubated at 55°C for 15 mins before treatments and then washed
537 with PBST (1xPBS/0.5x triton-X) between subsequent treatments. Tissues were treated
538 separately with trypsin (0.1% in 5%EDTA/1xPBS) and hyaluronidase (0.5% in 1xPBS/0.5x triton-
539 X) at 37°C for 15 mins each. The tissues were blocked with 4% goat serum/2% sheep/1xPBS for
540 1 hr, and then incubated overnight at 4°C with either Col2 antibody (1:100, II-II6B3, Hybridoma
541 Bank) or blocking solution (negative control). Secondary antibody labelling was done using 488-
542 conjugated goat anti-mouse antibody (1:1000, A32723 ThermoFisher Scientific) for 3 hours.

543

544 **Quantitative and statistical analyses**

545 Statistical analyses of TMDs were performed using SPSS V.22 (SPSS). Shapiro–Wilk test was
546 used to test for normal distribution of data. To assess differences among means, one-way

547 analysis of variance (ANOVA) was used followed by Tukey HSD or Games-Howell post hoc
548 analyses, depending upon whether homogeneity of variance assumption (Levene's test) was
549 met or not, respectively.
550

551 ## Data availability

552 Raw data from microCT projections and quantitative measurements have been deposited at
553 Dryad (DOI: 10.5061/dryad.crjdfn3b9) and can be accessed at
554 https://datadryad.org/stash/share/gnKH8kfRoKdHRE9rFGDausGzBZ1VTuCK3DB5gRPkrnp
555

556 ## Acknowledgements

557 This work was funded by Natural Sciences and Engineering Research Council (NSERC) grants
558 RGPIN 435655-201 and RGPIN 2014-05563 awarded to BFE. The authors are very thankful to
559 Adam Summers of Friday Harbor in the San Juan Islands for providing the spotted ratfish
560 samples and some feedback on the spotted ratfish data. Research described in this paper was
561 performed at the BMIT facility at the Canadian Light Source, which is supported by Canada
562 Foundation for Innovation, Natural Sciences and Engineering Research Council of Canada, the
563 University of Saskatchewan, Western Economic Diversification Canada, the National Research
564 Council Canada, and the Canadian Institutes of Health Research. We acknowledge the MRI
565 platform member of the national infrastructure France-BioImaging supported by the French
566 National Research Agency (ANR-10-INBS- 04, “Investments for the future”), the labex CEMEB
567 (ANR-10-LABX-0004) and NUMEV (ANR-10-LABX-0020).
568

569 **Figure legends**

570 **Figure 1. Mineralized tissues were abundant in the spotted ratfish, but they had lower tissue**
571 **mineral density (TMD) compared to the little skate and the small-spotted catshark.** (**A**)
572 Photograph of the ratfish *Hydrolagus colliei* illustrating the anterior region that was micro-CT
573 imaged. (**B-G**) Micro-CT 3D renderings of the anterior region of ratfish (B) showed mineralized
574 tissues in neural arches, basidorsals, and centra in segmented vertebrae (C,D), in the ceratohyal
575 and other skeletal elements in the pharyngeal skeleton (E), and in the fused vertebral synarcual
576 (F,G). (**H**) Comparative quantitative analyses showed that TMD of the synarcual, neural arch,
577 and centra in ratfish were significantly lower than TMDs of same regions in little skate and
578 catshark. Abbreviations: A, anterior; bb, basibranchial; bd, basidorsal; bh, basihyal; c, centrum
579 cb, ceratobranchial; ch, ceratohyal; D, dorsal; hbs, hypobranchials; L, left; MK, Meckel's; na,
580 neural arch; P, posterior; R, right; snf, spinal nerve foramina; V, ventral. * indicates statistically
581 significant comparison ($p<0.05$). Scale bars: as indicated.

582

583 **Figure 2. Ratfish lack neural arch bone-like tissue.** (**A-C**) Micro-CT 3D renderings showed a
584 non-continuous pattern of mineralized tissues in neural arches of segmented vertebrae in
585 ratfish (A), compared to the continuous mineralization pattern of compact, bone-like tissue in
586 catshark (B) and little skate (C). (**D-F**) Micro-CT 2D virtual slices showed that mineralized tissues
587 (arrows) in ratfish neural arches were restricted to medial and lateral peripheries (D), whereas
588 the bone-like tissue in catshark and little skate extended much deeper in the neural arch (E,F).
589 (**G-I**) Alizarin red staining of histological sections confirmed micro-CT representation of
590 mineralization patterns in ratfish (G), catshark (H), and little skate (I) neural arches, and Alcian

591 blue revealed cartilaginous regions. (**J-L**) Picrosirius red staining did not reveal birefringent
592 collagen fibers in ratfish neural arches (J), but such staining was abundant in bone-like tissues in
593 catshark (K) and little skate (L). Birefringent fibers (likely reticular) were present in muscles
594 (vertical arrows) on the lateral sides of neural arches in all species. Col2 immunostaining
595 confirmed Alcian blue staining, identifying cartilage regions in all species. The neural arch core
596 in catshark (K) and little skate (L) consisted of mostly unmineralized cartilage and mineralized
597 cartilage, respectively. Abbreviations: 2D, two-dimensional; 3D, three-dimensional; Ab, Alcian
598 blue; Ar, Alizarin red; BLT, bone-like tissue; c, cartilage; Col2, collagen type 2; D, dorsal; IF,
599 immunofluorescence; L, lateral; M, medial; MC, mineralized cartilage; PSR, picrosirius red; V,
600 ventral. Scale bars: as indicated.
601
602 **Figure 3. Ratfish, catshark, and little skate all showed trabecular mineralization, but ratfish**
603 **and catshark did not have a bone-like cap zone.** (**A-H**) Micro-CT renderings of the ratfish
604 ceratohyal (A,E) and catshark caudal vertebra (B,F) demonstrated non-tesseral trabecular
605 mineralization, while little skate hyomandibula had tesseral trabecular mineralization (C,G).
606 Little skate precaudal vertebra had tesseral polygonal mineralization (D,H) overlying tesseral
607 trabecular mineralization (H'). Regions for hi-mag views in panels E-H' are indicated in
608 corresponding panels of A-D. (**I-P**) Alcian blue/Alizarin red and Safranin O/fast green staining of
609 histological sections demonstrated that the body zone of non-tesseral or tesseral trabecular
610 mineralized tissues in ratfish (I,M), catshark (J,N), and little skate (K,L,O,P) was mineralized
611 cartilage, while the cap zone of tesseral polygonal mineralization was bone-like (K,L,O,P). (**Q-T**)
612 Col2 immunostaining of adjacent sections to panels I-P confirmed cartilage regions in all

613 species, while picrosirius red staining confirmed the bone-like tesseral cap zone in little skate.
614 Abbreviations: Ab, Alcian blue; Ar, Alizarin red; Bz, body zone; c, cartilage; Col2, collagen type 2;
615 Cz, cap zone; D, dorsal; IF, immunofluorescence; L, lateral; M, medial; PSR, picrosirius red; NA,
616 neural arch; NS, neural spine; V, ventral. Scale bars: as indicated.
617
618 **Figure 4. Micro-CT segmentation clearly correlated histological features and mineralization**
619 **patterns.** (**A-C**) Trichrome staining showed that spokes in the body zone of ratfish non-tesseral
620 trabeculae (A) or little skate trabecular (B) or polygonal (C) tesserae had low cellularity and
621 were unstained, while intense acid fuchsin staining marked the smaller and larger cap zones of
622 little skate trabecular (B) and polygonal (C) tesserae, respectively. (**D-I**) 3D renderings of
623 synchrotron micro-CT data showed that hypermineralized spokes (*, segmented in blue) were
624 in the body zone of ratfish non-tesseral trabeculae (D,G) or little skate trabecular (E,H) or
625 polygonal (F,I) tesserae. Tesseral cap zones could also be segmented clearly (red) in little skate
626 (E,F,H,I). (**J-O**) Segmented 3D renderings demonstrated that spokes in ratfish were patchy in
627 deep (J) or superficial (M) views, while little skate spokes displayed a radiating pattern
628 traversing most of the trabecular patterns in either trabecular (K,N) or polygonal (L,O) tesserae.
629 The smaller cap zone in trabecular tesserae (N) was not laterally extensive enough to display a
630 superficial polygonal pattern like that of polygonal tesserae (O). Abbreviations: Bz, body zone;
631 Cz, cap zone. Scale bars: as indicated.
632
633 **Figure 5. Ratfish centra had the same features as areolar mineralized tissues in little skate**
634 **and catshark.** (**A-C**) Micro-CT renderings demonstrated that centra in ratfish (A), catshark (B),

635 and little skate (C) all had a compact mineralization, but ratfish centra were organized in
636 multiple rings and did not display the gross biconcave morphology seen in catshark or little
637 skate. (**D-O**) Alcian blue/Alizarin red and Safranin O section histology and Col2 immunostaining
638 demonstrated that mineralized centra in ratfish (D,G,J), catshark (E,H,K), and little skate (F,I,L)
639 all comprised a middle layer with elongate lacunae in concentric lamellae, but in ratfish this was
640 mineralized cartilage, while catshark and little skate had little to no Safranin O or Col2 staining,
641 respectively, in this region. Catshark mineralized centra also comprised the outer layer, while
642 little skate mineralized centra also comprised both inner and outer layers. These additional
643 centra layers had rounded cells embedded in matrix of weak Safranin O staining and Col2
644 immunofluorescence. Regions for hi-mag views in panels G-O are indicated in corresponding
645 panels of D-F; regions for hi-mag inserts in panels G-I are indicated in those panels.
646 Abbreviations: A, anterior; Ab, Alcian blue; Ar, Alizarin red; c, cartilage; Col2, collagen type 2; D,
647 dorsal; IF, immunofluorescence; IL, inner layer; L, lateral; M, medial, OL, outer layer; P,
648 posterior; V, ventral. Scale bars: as indicated; inserts in G-I are 20 µm.
649
650 **Figure 6. Morphological and histological features of centra were shared between little skate**
651 **embryos and juveniles and adult ratfish.** (**A-D**) Desktop micro-CT renderings showed centra
652 and other mineralized structures in vertebral segments (dashed lines) of little skate embryos
653 and juveniles (A-C) and adult ratfish (D). (**E-H**) Synchrotron micro-CT renderings of centra in
654 little skate embryos and juveniles (E-G) and adult ratfish (H) showed that centra in the ratfish
655 were slightly constricted, like those of little skate embryos (red arrows). (**I-K**) Alcian
656 blue/Alizarin red section histology showed that areolar mineralized tissue constituted the only

657 centra layer in little skate embryos (I,J), whereas an outer mineralized centra layer was present
658 in 6.5 cm DW juveniles (K). (**L**) Tissue mineral density (TMD) of centra in ratfish was similar to
659 those of stage 33 embryos and 6.5 cm DW juveniles of little skate. Abbreviation: A, anterior; Ab,
660 Alcian blue; Ar, Alizarin red; bd, basidorsal; C, centrum; HA, haemal arch; L, lateral; M, medial;
661 NA, neural arch; OL, outer layer; P, posterior.* indicates statistically significant comparison
662 (p<0.05). Scale bars: as indicated.
663
664 **Figure 7. Character states of mineralized tissues in various extant and fossil chondrichthyan**
665 **species suggest shared and derived features.** Non-tesseral trabecular mineralization (NTT) is
666 likely a symplesiomorphic (shared ancestral) character of stem and crown chondrichthyans,
667 because it is pervasive in fossil and extant chondrichthyans. Polygonal (PT) and trabecular (TT)
668 tesseral mineralization patterns appear to be absent in extant holocephalans and stem
669 chondrichthyans, but their presence in some extant elasmobranchs and a fossil holocephalan
670 suggest that these tesseral mineralizations are synapomorphic (shared derived) characters of
671 crown chondrichthyans, subsequently lost in extant holocephalans. Areolar (AR) mineralized
672 tissue is present in extant elasmobranchs and holocephalans, but its absence in stem
673 chondrichthyans suggests that it is a synapomorphic character of crown chondrichthyans. The
674 absence of neural arch bone-like tissue (BLT) in holocephalans further supports the conclusion
675 that it is a synapomorphic character of elasmobranchs. The presence of a histological body zone
676 (BZ) in either tesseral or non-tesseral mineralized tissues of stem and crown chondrichthyans
677 suggests that the body zone is a symplesiomorphic character of all chondrichthyans. The
678 histological cap zone (CZ) in some elasmobranchs, along with the inference that polygonal

679 tesserae in a fossil holocephalan means that they had cap zones, suggests that the cap zone is
680 also a synapomorphic character of crown chondrichthyans. 0, 1, and ? indicate absence,
681 presence, and unknown, respectively, of characters for the listed species. See Supplemental
682 Table 2 for downloadable character matrix.

683

684 **References**

685 Arratia, G., Schultze, H.P., Casciotta, J., 2001. Vertebral column and associated elements in dipnoans and
686 comparison with other fishes: development and homology. J Morphol 250, 101-172 DOI:
687 10.1002/jmor.1062.

688 Ashique, A.M., Atake, O.J., Ovens, K., Guo, R., Pratt, I.V., Detrich III, H.W., Cooper, D.M., Desvignes, T.,
689 Postlethwait, J.H., Eames, B.F., 2022. Bone microstructure and bone mineral density are not systemically
690 different in Antarctic icefishes and related Antarctic notothenioids. Journal of Anatomy 240, 34-49 DOI:
691 https://doi.org/10.1111/joa.13537.

692 Atake, O.J., Cooper, D.M.L., Eames, B.F., 2019. Bone-like features in skate suggest a novel elasmobranch
693 synapomorphy and deep homology of trabecular mineralization patterns. Acta Biomater 84, 424-436
694 DOI: 10.1016/j.actbio.2018.11.047.

695 Atake, O.J., Eames, B.F., 2021. Mineralized Cartilage and Bone-Like Tissues in Chondrichthyans Offer
696 Potential Insights Into the Evolution and Development of Mineralized Tissues in the Vertebrate
697 Endoskeleton. Frontiers in Genetics 12 DOI: 10.3389/fgene.2021.762042.

698 Berio, F., Broyon, M., Enault, S., Pirot, N., López-Romero, F.A., Debiais-Thibaud, M., 2021. Diversity and
699 Evolution of Mineralized Skeletal Tissues in Chondrichthyans. Frontiers in Ecology and Evolution 9, 223
700 DOI: 10.3389/fevo.2021.660767.

701 Bordat, C., 1987. Étude ultrastructurale de l'os des vertèbres du Sélacien Scyliorhinus canicula L.
702 Canadian Journal of Zoology 65, 1435-1444 DOI: 10.1139/z87-226.

703 Claeson, K.M., 2011. The synarcual cartilage of batoids with emphasis on the synarcual of Rajidae. J
704 Morphol 272, 1444-1463 DOI: 10.1002/jmor.10996.

705 Clement, J., 1992. Re-examination of the fine structure of endoskeletal mineralization in
706 chondrichthyans: implications for growth, ageing and calcium homeostasis. Marine and Freshwater
707 Research 43, 157-181.

708 Coates, M.I., Finarelli, J.A., Sansom, I.J., Andreev, P.S., Criswell, K.E., Tietjen, K., Rivers, M.L., La Riviere,
709 P.J., 2018. An early chondrichthyan and the evolutionary assembly of a shark body plan. Proc Biol Sci
710 285, 20172418 DOI: 10.1098/rspb.2017.2418.

711 Criswell, K.E., Coates, M.I., Gillis, J.A., 2017. Embryonic development of the axial column in the little
712 skate, *Leucoraja erinacea*. J Morphol 278, 300-320 DOI: 10.1002/jmor.20637.

713 Criswell, K.E., Gillis, J.A., 2020. Resegmentation is an ancestral feature of the gnathostome vertebral
714 skeleton. Elife 9, e51696 DOI: 10.7554/eLife.51696.

715 Daniel, J.F., 1934. The elasmobranch fishes. University of California press, Berkeley, California.

716 Dean, M.N., Bizzarro, J.J., Clark, B., Underwood, C.J., Johanson, Z., 2017. Large batoid fishes frequently
717 consume stingrays despite skeletal damage. Royal Society Open Science 4, 170674 DOI:
718 doi:10.1098/rsos.170674.

719 Dean, M.N., Summers, A.P., 2006. Mineralized cartilage in the skeleton of chondrichthyan fishes.
720 Zoology (Jena) 109, 164-168 DOI: 10.1016/j.zool.2006.03.002.

721 Debiais-Thibaud, M., 2018. The Evolution of Endoskeletal Mineralisation in Chondrichthyan Fish,
722 Evolution and development of fishes. Cambridge University Press, pp. 110-125.

723 Debiais-Thibaud, M., 2019. The Evolution of Endoskeletal Mineralisation in Chondrichthyan Fish:
724 Development, Cells and Molecules, in: Underwood, C., Richter, M., Johanson, Z. (Eds.), Evolution and
725 Development of Fishes. Cambridge University Press, Cambridge, pp. 110-125.

726 Didier, D.A., 1995. Phylogenetic systematics of extant chimaeroid fishes (Holocephali, Chimaeroidei).
727 American Museum of Natural History, New York.

728 Eames, B.F., Allen, N., Young, J., Kaplan, A., Helms, J.A., Schneider, R.A., 2007. Skeletogenesis in the swell
729 shark *Cephaloscyllium ventriosum*. J Anat 210, 542-554 DOI: 10.1111/j.1469-7580.2007.00723.x.

730 Eames, B.F., Yan, Y.-L., Swartz, M.E., Levic, D.S., Knapik, E.W., Postlethwait, J.H., Kimmel, C.B., 2011.
731 Mutations in fam20b and xylt1 reveal that cartilage matrix controls timing of endochondral ossification
732 by inhibiting chondrocyte maturation. PLoS Genetics 7, e1002246 DOI: 10.1371/journal.pgen.1002246.

733 Enault, S., Munoz, D.N., Silva, W.T., Borday-Birraux, V., Bonade, M., Oulion, S., Venteo, S., Marcellini, S.,
734 Debiais-Thibaud, M., 2015. Molecular footprinting of skeletal tissues in the catshark *Scyliorhinus*
735 *canicula* and the clawed frog *Xenopus tropicalis* identifies conserved and derived features of vertebrate
736 calcification. Front Genet 6, 283 DOI: 10.3389/fgene.2015.00283.

737 Ferguson, C.M., Miclau, T., Hu, D., Alpern, E., Helms, J.A., 1998. Common molecular pathways in skeletal
738 morphogenesis and repair. Ann N Y Acad Sci 857, 33-42 DOI: 10.1111/j.1749-6632.1998.tb10105.x.

739 Forbes, G.B., 1976. Calcium accumulation by the human fetus. Pediatrics 57, 976-977 DOI:
740 10.1542/peds.57.6.976.

741 Frey, L., Coates, M., Ginter, M., Hairapetian, V., Rucklin, M., Jerjen, I., Klug, C., 2019. The early
742 elasmobranch *Phoebodus*: phylogenetic relationships, ecomorphology and a new time-scale for shark
743 evolution. Proc Biol Sci 286, 20191336 DOI: 10.1098/rspb.2019.1336.

744 Gadow, H.F., Abbott, E., 1895. IV. On the evolution of the vertebral column of fishes. Philosophical
745 Transactions of the Royal Society of London. (B.) 186, 163-221 DOI: 10.1098/rstb.1895.0004.

746 Garstang, W., 1922. The Theory of Recapitulation: A Critical Re-statement of the Biogenetic Law.
747 Zoological Journal of the Linnean Society 35, 81-101 DOI: 10.1111/j.1096-3642.1922.tb00464.x.

748 Gillis, J.A., Rawlinson, K.A., Bell, J., Lyon, W.S., Baker, C.V., Shubin, N.H., 2011. Holocephalan embryos
749 provide evidence for gill arch appendage reduction and opercular evolution in cartilaginous fishes. Proc
750 Natl Acad Sci U S A 108, 1507-1512 DOI: 10.1073/pnas.1012968108.

751 Goldring, M.B., Tsuchimochi, K., Ijiri, K., 2006. The control of chondrogenesis. J Cell Biochem 97, 33-44
752 DOI: 10.1002/jcb.20652.

753 Golub, E.E., 2009. Role of matrix vesicles in biomineralization. Biochim Biophys Acta 1790, 1592-1598
754 DOI: 10.1016/j.bbagen.2009.09.006.

Herbert, A.M., Dean, M.N., Summers, A.P., Wilga, C.D., 2022. Biomechanics of the jaws of spotted ratfish. Journal of Experimental Biology 225 DOI: 10.1242/jeb.243748.

Janvier, P., 1996. Early vertebrates. Oxford University Press.

Jayasankar, A.K., Seidel, R., Hosny, A., Weaver, J.C., Fratzl, P., Chen, J., Dean, M.N., 2020. Multi-scale modeling and mechanical performance characterization of stingray skeleton-inspired tessellations. Journal of the Mechanics and Physics of Solids 138, 103906 DOI: 10.1016/j.jmps.2020.103906.

Johanson, Z., Boisvert, C., Maksimenko, A., Currie, P., Trinajstic, K., 2015. Development of the Synarcual in the Elephant Sharks (Holocephali; Chondrichthyes): Implications for Vertebral Formation and Fusion. PLoS One 10, e0135138 DOI: 10.1371/journal.pone.0135138.

Johanson, Z., Trinajstic, K., Carr, R., Ritchie, A., 2012. Evolution and development of the synarcual in early vertebrates. Zoomorphology 132, 95-110 DOI: 10.1007/s00435-012-0169-9.

Junqueira, L.C., Cossermelli, W., Brentani, R., 1978. Differential staining of collagens type I, II and III by Sirius Red and polarization microscopy. Arch Histol Jpn 41, 267-274 DOI: 10.1679/aohc1950.41.267.

Kemp, N.E., Westrin, S.K., 1979. Ultrastructure of calcified cartilage in the endoskeletal tesserae of sharks. J Morphol 160, 75-109 DOI: 10.1002/jmor.1051600106.

Kölliker, A., 1860. Über das Ende der Wirbelsäule der Ganoiden und einiger Teleostier. W. Engelmann.

Liem, K.F., Bemis, Willam E, Walker, Warren F, and Grande, Lance, 2001. Functional anatomy of the vertebrates: an evolutionary perspective, Third ed. Brooks/Cole, Belmont, CA.

Lowenstam, H.A., 1981. Minerals formed by organisms. Science 211, 1126-1131 DOI: 10.1126/science.7008198.

Maisey, J.G., 2013. The diversity of tessellated calcification in modern and extinct chondrichthyans. Revue de Paléobiologie 32, 355-371.

Maisey, J.G., Denton, J.S.S., Burrow, C., Pradel, A., 2021. Architectural and ultrastructural features of tessellated calcified cartilage in modern and extinct chondrichthyan fishes. J Fish Biol 98, 919-941 DOI: 10.1111/jfb.14376.

Marramà, G., Schultz, O., Kriwet, J., 2019. A new Miocene skate from the Central Paratethys (Upper Austria): the first unambiguous skeletal record for the Rajiformes (Chondrichthyes: Batomorphii). J Syst Palaeontol 17, 937-960 DOI: 10.1080/14772019.2018.1486336.

Maxwell, E.E., Fröbisch, N.B., Heppleston, A.C., 2008. Variability and Conservation in Late Chondrichthyan Development: Ontogeny of the Winter Skate (Leucoraja ocellata). The Anatomical Record 291, 1079-1087 DOI: https://doi.org/10.1002/ar.20719.

Miles, R.S., 1970. Remarks on the Vertebral Column and Caudal Fin of Acanthodian Fishes. Lethaia 3, 343-362 DOI: 10.1111/j.1502-3931.1970.tb00828.x.

Omelon, S., Georgiou, J., Variola, F., Dean, M.N., 2014. Colocation and role of polyphosphates and alkaline phosphatase in apatite biomineralization of elasmobranch tesserae. Acta Biomater 10, 3899-3910 DOI: 10.1016/j.actbio.2014.06.008.

Ørvig, T., 1951. The endoskeleton, with remarks on the hard tissues of lower vertebrates in general, Histologic studies of Placoderms and fossil Elasmobranchs. Almqvist & Wiksell, Stockholm, pp. 321-454.

Pears, J.B., Johanson, Z., Trinajstic, K., Dean, M.N., Boisvert, C.A., 2020. Mineralization of the *Callorhinchus* Vertebral Column (Holocephali; Chondrichthyes). Front Genet 11, 571694 DOI: 10.3389/fgene.2020.571694.

Peignoux-Deville, J., Lallier, F., Vidal, B., 1982. Evidence for the presence of osseous tissue in dogfish vertebrae. Cell Tissue Res 222, 605-614 DOI: 10.1007/BF00213858.

Porter, M.E., Beltrán, J.L., Koob, T.J., Summers, A.P., 2006. Material properties and biochemical composition of mineralized vertebral cartilage in seven elasmobranch species (Chondrichthyes). J Exp Biol 209, 2920-2928 DOI: 10.1242/jeb.02325.

Ridewood, W., MacBride, E.W., 1921. VIII.—On the calcification of the vertebral centra in sharks and rays. Philosophical Transactions of the Royal Society of London. Series B, Containing Papers of a Biological Character 210, 311-407 DOI: 10.1098/rstb.1921.0008.

Rossert, J., de Crombrugghe, B., 2002. Type I collagen: structure, synthesis, and regulation, Principles of bone biology. Elsevier, pp. 189-XVIII.

Seidel, R., Blumer, M., Chaumel, J., Amini, S., Dean, M.N., 2020. Endoskeletal mineralization in chimaera and a comparative guide to tessellated cartilage in chondrichthyan fishes (sharks, rays and chimaera). J R Soc Interface 17, 20200474 DOI: 10.1098/rsif.2020.0474.

Seidel, R., Blumer, M., Pechriggl, E.J., Lyons, K., Hall, B.K., Fratzl, P., Weaver, J.C., Dean, M.N., 2017. Calcified cartilage or bone? Collagens in the tessellated endoskeletons of cartilaginous fish (sharks and rays). J Struct Biol 200, 54-71 DOI: 10.1016/j.jsb.2017.09.005.

Seidel, R., Lyons, K., Blumer, M., Zaslansky, P., Fratzl, P., Weaver, J.C., Dean, M.N., 2016. Ultrastructural and developmental features of the tessellated endoskeleton of elasmobranchs (sharks and rays). J Anat 229, 681-702 DOI: 10.1111/joa.12508.

Smith, M., Manzanares, E., Underwood, C., Healy, C., Clark, B., Johanson, Z., 2020. Holocephalan (Chondrichthyes) dental plates with hypermineralized dentine as a substitute for missing teeth through developmental plasticity. J Fish Biol 97, 16-27 DOI: 10.1111/jfb.14302.

Smith, M.M., Hall, B.K., 1990. Development and evolutionary origins of vertebrate skeletogenic and odontogenic tissues. Biol Rev Camb Philos Soc 65, 277-373 DOI: 10.1111/j.1469-185x.1990.tb01427.x.

Stehmann, M.F., 2002. Proposal of a maturity stages scale for oviparous and viviparous cartilaginous fishes (Pisces, Chondrichthyes). Archive of Fishery and Marine research 50, 23-48.

Vazquez, D.M., Díaz de Astarloa, J.M., Gabbanelli, V., Mabragaña, E., 2020. Comparative embryonic development patterns in three deep-water skates from the southwest Atlantic. Deep Sea Research Part I: Oceanographic Research Papers 161, 103301 DOI: 10.1016/j.dsr.2020.103301.

Venkatesh, B., Lee, A.P., Ravi, V., Maurya, A.K., Lian, M.M., Swann, J.B., Ohta, Y., Flajnik, M.F., Sutoh, Y., Kasahara, M., Hoon, S., Gangu, V., Roy, S.W., Irimia, M., Korzh, V., Kondrychyn, I., Lim, Z.W., Tay, B.-H., Tohari, S., Kong, K.W., Ho, S., Lorente-Galdos, B., Quilez, J., Marques-Bonet, T., Raney, B.J., Ingham, P.W., Tay, A., Hillier, L.W., Minx, P., Boehm, T., Wilson, R.K., Brenner, S., Warren, W.C., 2014. Elephant shark genome provides unique insights into gnathostome evolution. Nature 505, 174-179 DOI: 10.1038/nature12826.

Wilga, C.A.D., Ferry, L.A., 2015. 4 - Functional Anatomy and Biomechanics of Feeding in Elasmobranchs, in: Shadwick, R.E., Farrell, A.P., Brauner, C.J. (Eds.), Fish Physiology. Academic Press, pp. 153-187.

Wurmbach, H., 1932. Das Wachstum des Selachierwirbels und seiner Gewebe. Zool Jahrb (Abt Anat Ont Tiere) 55, 1-136.

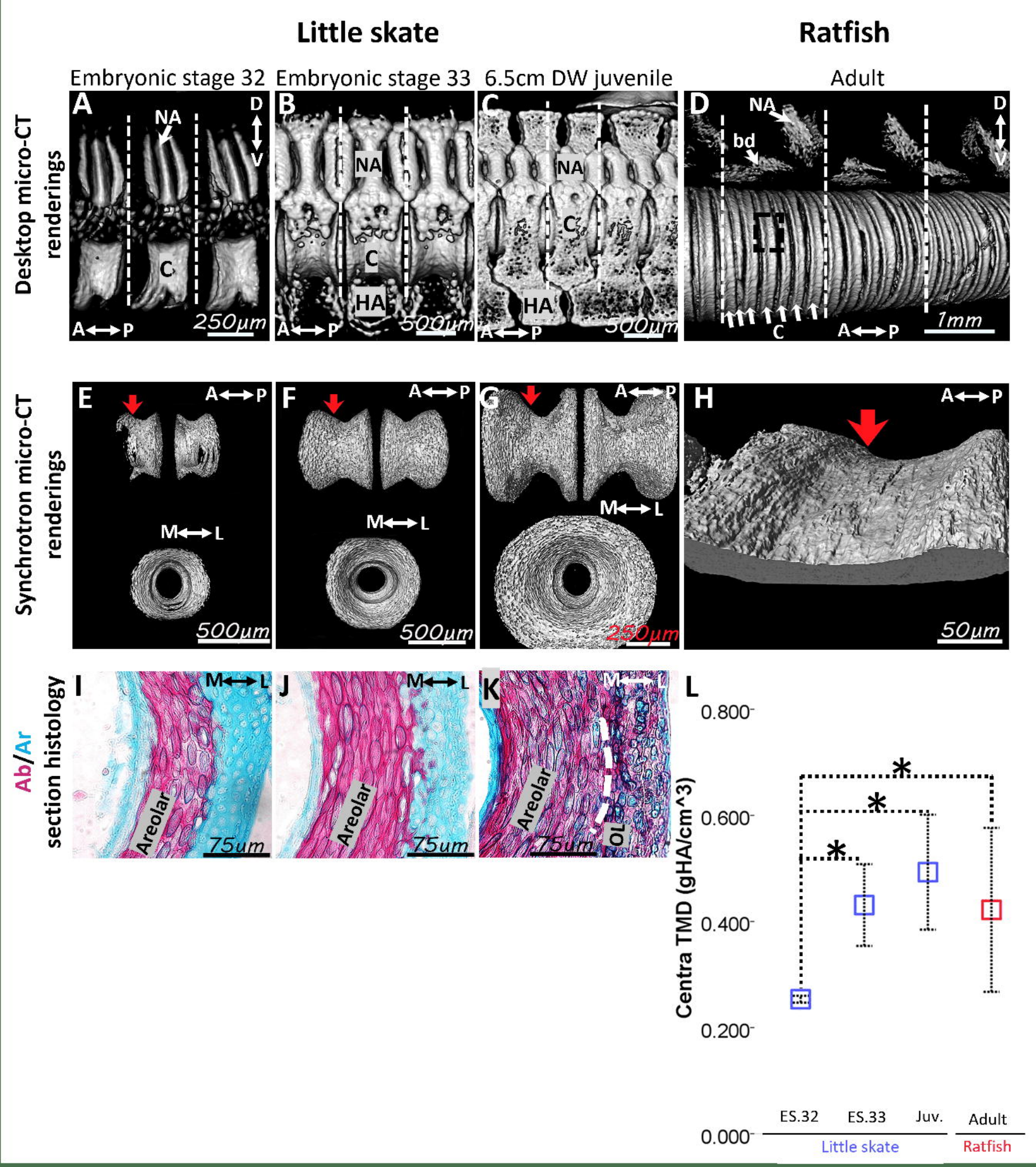
Little skate
Ratfish
Embryonic stage 32
Embryonic stage 33
6.5cm DW juvenile
Adult
Desktop micro-CT renderings
A
NA
D
V
C
A↔P
250µm
B
NA
C
HA
A↔P
500µm
C
NA
C
HA
A↔P
500µm
D
NA
bd
D
V
C
A↔P
1mm
Synchrotron micro-CT renderings
E
A↔P
M↔L
500µm
F
A↔P
M↔L
500µm
G
A↔P
M↔L
250µm
H
A↔P
50µm
Ab/Ar section histology
I
M↔L
Areolar
75um
J
M↔L
Areolar
75um
K
M↔L
Areolar
OL
75um
L
Centra TMD (gHA/cm^3)
0.800
0.600
0.400
0.200
0.000
*
*
*
ES.32
ES.33
Juv.
Adult
Little skate
Ratfish

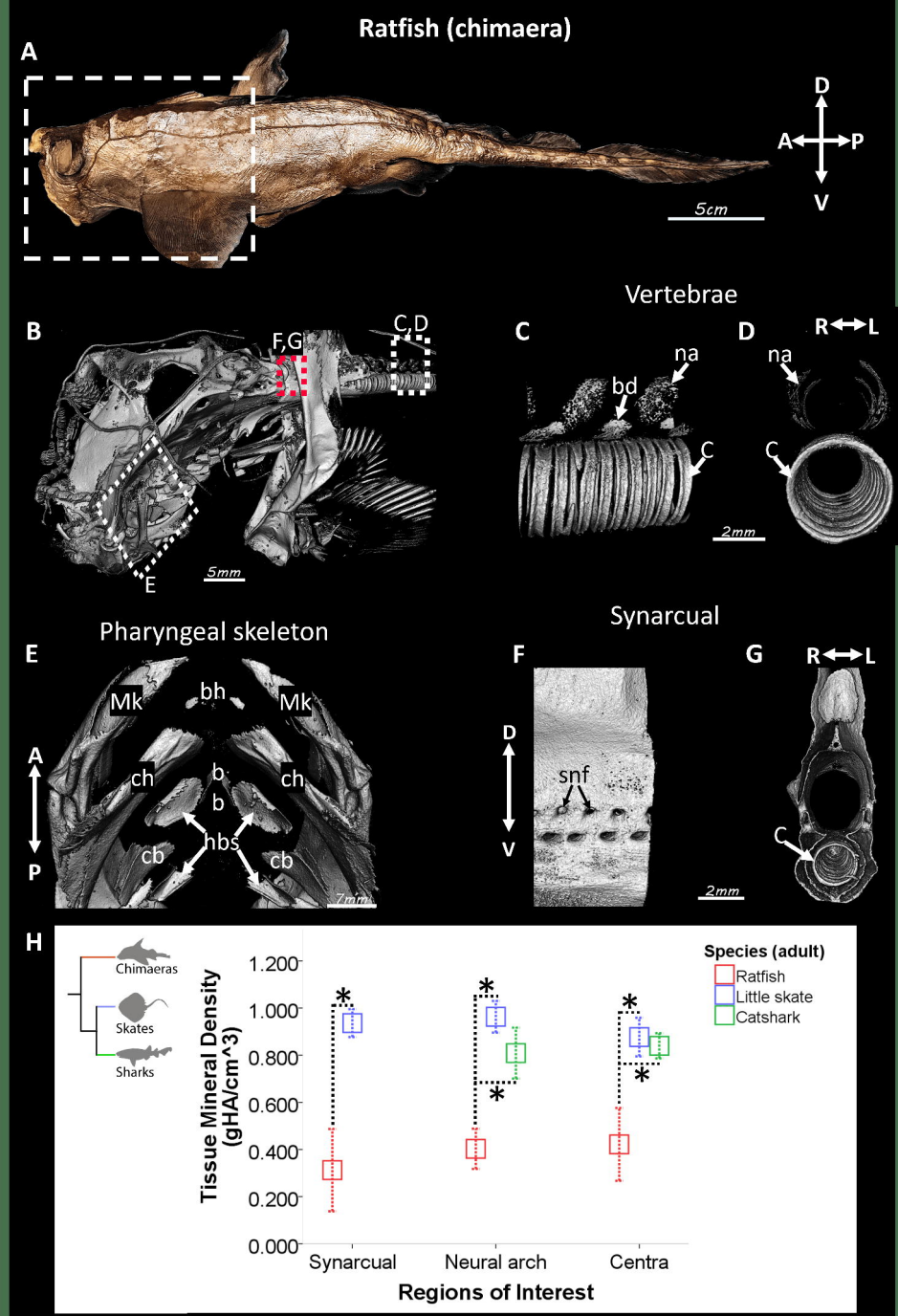
Ratfish (chimaera)
A
D
A
P
V
5cm
B
F,G
C,D
E
5mm
Vertebrae
C
na
bd
C
2mm
D
R
L
na
C
Pharyngeal skeleton
E
Mk
bh
Mk
A
P
ch
b
b
ch
hbs
cb
cb
7mm
Synarcual
F
D
V
snf
2mm
G
R
L
C
H
Chimaeras
Skates
Sharks
Tissue Mineral Density (gHA/cm^3)
1.200
1.000
0.800
0.600
0.400
0.200
0.000
Synarcual
Neural arch
Centra
Regions of Interest
Species (adult)
Ratfish
Little skate
Catshark

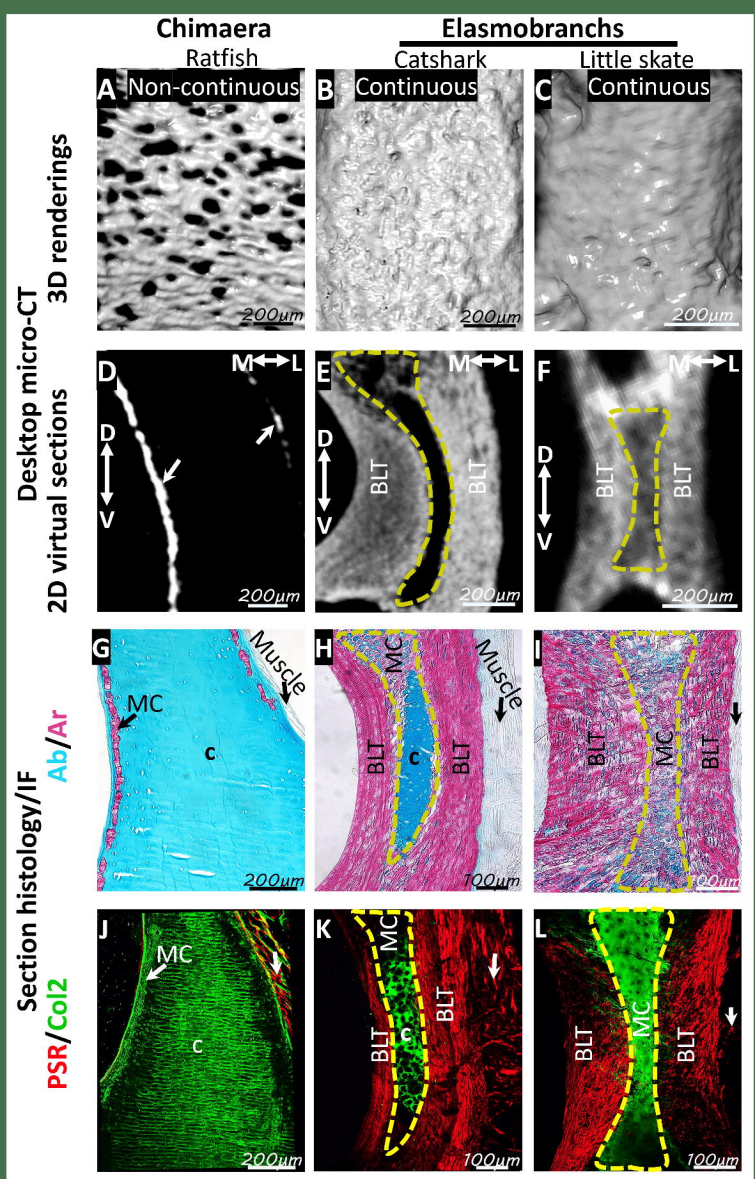

Chimaera
Ratfish
Elasmobranchs
Catshark
Little skate
Desktop micro-CT
3D renderings
2D virtual sections
Section histology/IF
Ab/Ar
PSR/Col2
A Non-continuous
B Continuous
C Continuous
D
E
F
M↔L
D
V
BLT
G
H
I
J
K
L
MC
c
Muscle
200µm
100µm

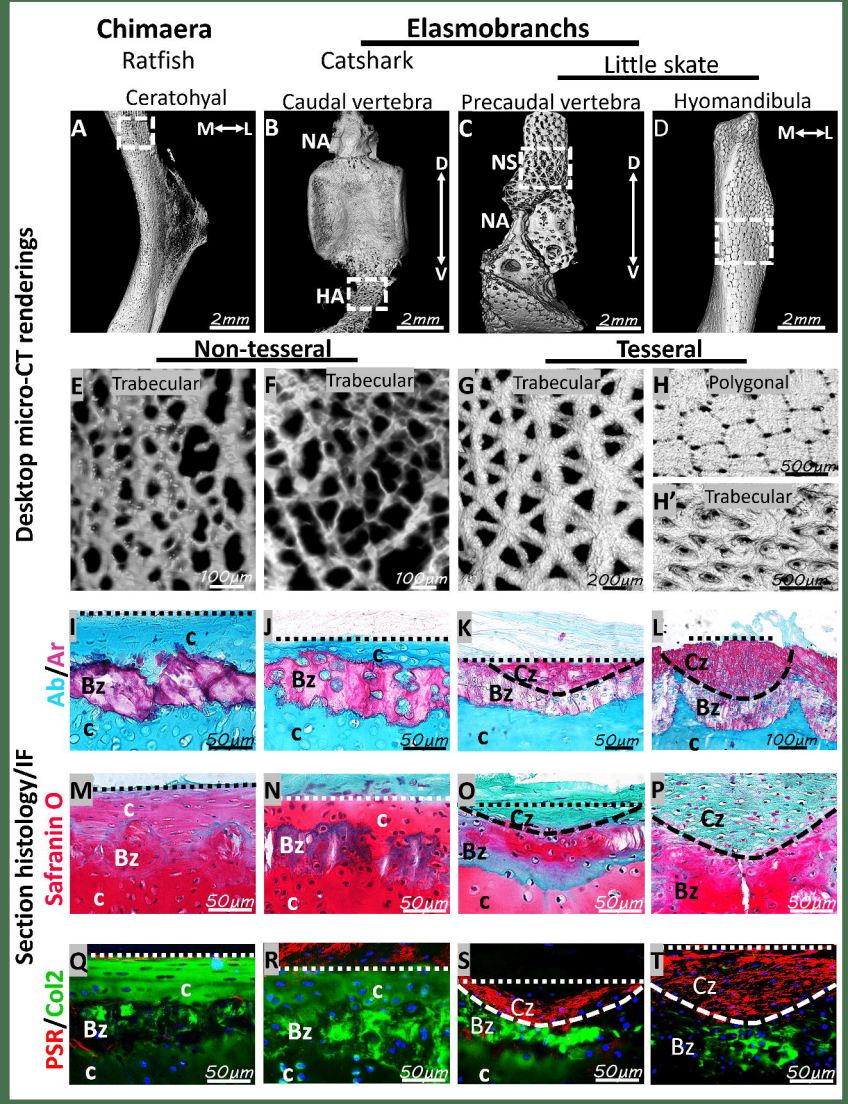
Chimaera
Ratfish
Elasmobranchs
Catshark
Little skate
Ceratohyal
Caudal vertebra
Precaudal vertebra
Hyomandibula
Desktop micro-CT renderings
A
M↔L
2mm
B
NA
HA
D
V
2mm
C
NS
NA
D
V
2mm
D
M↔L
2mm
Non-tesseral
Tesseral
E
Trabecular
100µm
F
Trabecular
100µm
G
Trabecular
200µm
H
Polygonal
500µm
H'
Trabecular
500µm
Section histology/IF
Ab/Ar
I
c
Bz
c
50µm
J
c
Bz
c
50µm
K
Cz
Bz
c
50µm
L
Cz
Bz
c
100µm
Safranin O
M
c
Bz
c
50µm
N
c
Bz
c
50µm
O
Cz
Bz
c
50µm
P
Cz
Bz
50µm
PSR/Col2
Q
c
Bz
c
50µm
R
c
Bz
c
50µm
S
Cz
Bz
c
50µm
T
Cz
Bz
50µm

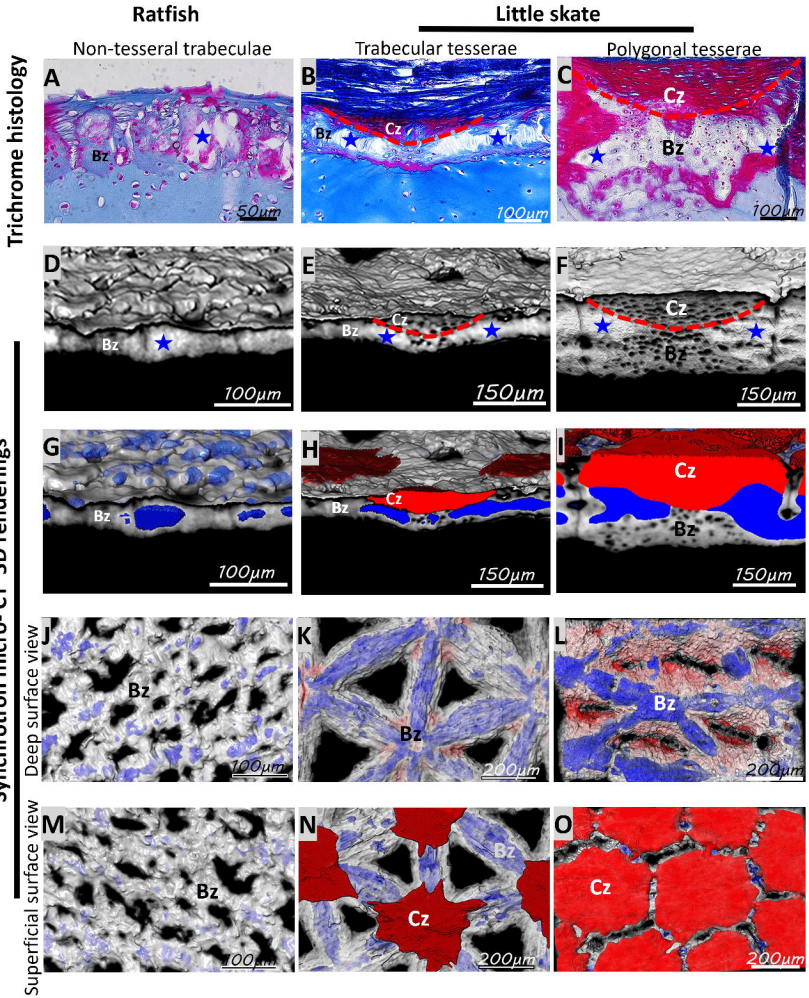
Ratfish
Little skate
Non-tesseral trabeculae
Trabecular tesserae
Polygonal tesserae
Trichrome histology
Synchrotron micro- CT 3D renderings
Deep surface view
Superficial surface view
A
B
C
D
E
F
G
H
I
J
K
L
M
N
O
Bz
Cz
50µm
100µm
150µm
200µm

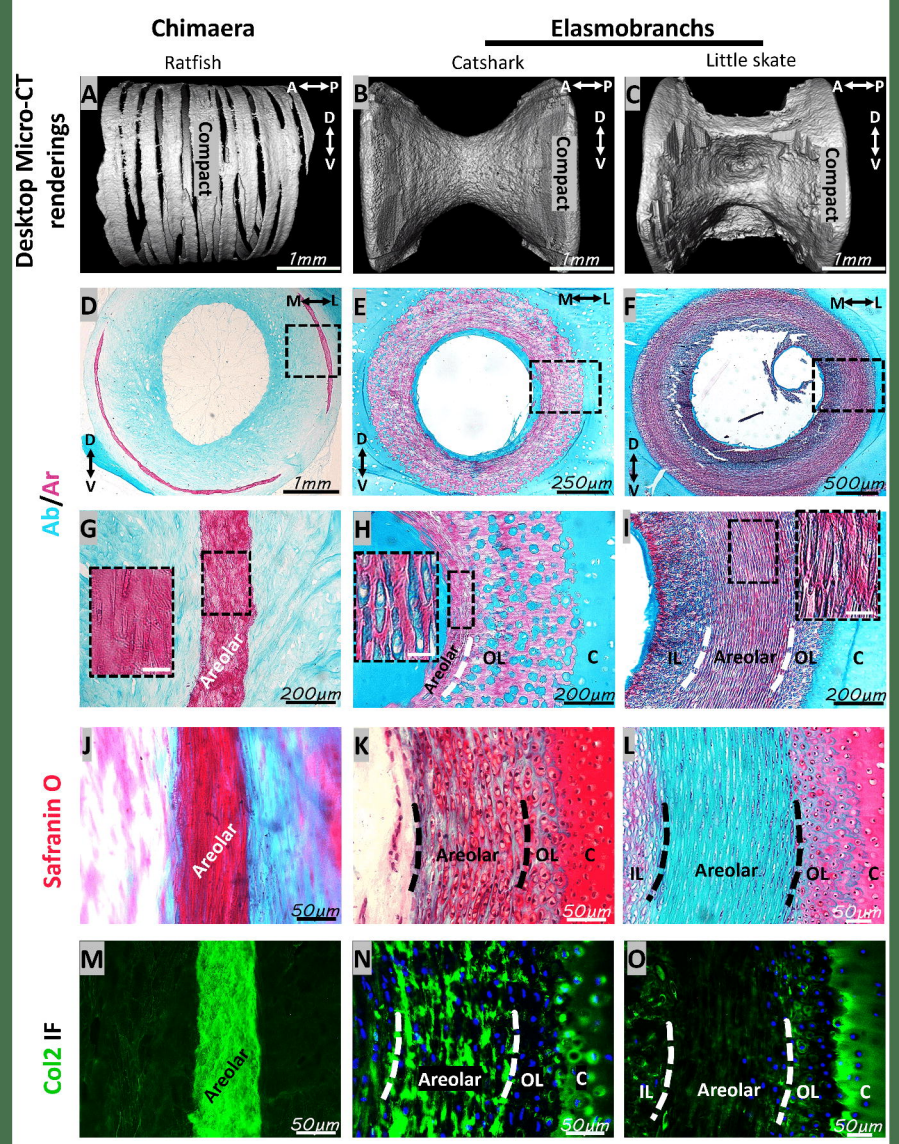
Chimaera
Elasmobranchs
Ratfish
Catshark
Little skate
Desktop Micro-CT renderings
Ab/Ar
Safranin O
Col2 IF
A
B
C
D
E
F
G
H
I
J
K
L
M
N
O
A↔P
D↕V
M↔L
Compact
1mm
250µm
500µm
200µm
50µm
Areolar
OL
C
IL

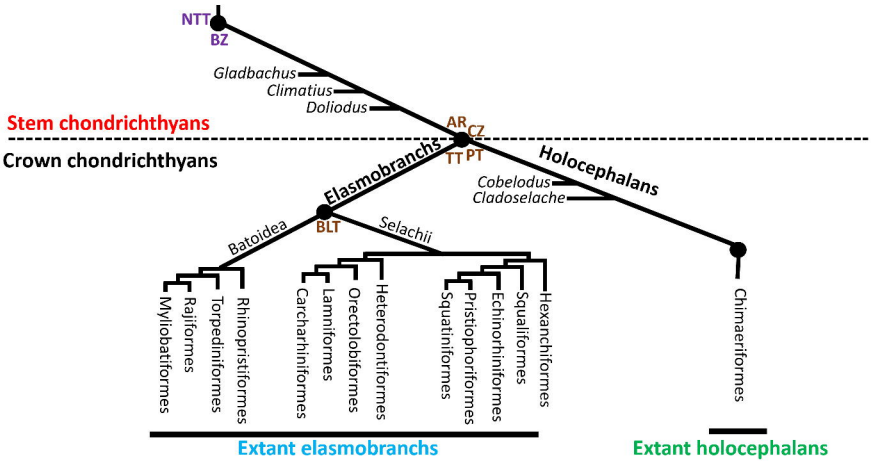

	NTT	BZ	AR	CZ	TT	PT	BLT
Gladbachus	1	1	0	0	0	0	?
Climatius	1	1	0	0	0	0	?
Doliodus	1	1	0	0	0	0	?
Cobelodus	?	1	?	1	1	1	?
Cladoselache	1	1	?	0	0	0	?
Rhinopristiformes (*P. productus, R. ancylostoma*)	0	1	1	1	1	1	0
Torpediniformes (*Torpedo* sp, *N. bancroftii, T. californica*)	0	1	1	1	1	1	1
Myliobatiformes (*G. micrura, U. halleri, D. sabina, M. californica, R. bonasus*)	0	1	1	1	1	1	0
Rajiformes (*R. clavata, L. erinacea, A. radiata, P. violacea, R. stellulata, R. eglanteria, B. eatonii*)	0	1	1	1	1	1	1
Heterodontiformes (*H. francisci*)	1	1	1	0	0	0	1
Orectolobiformes (*C. punctatum*)	?	1	1	?	?	?	1
Lamniformes (*C. taurus*)	?	1	1	1	1	1	0
Carcharhiniformes (*G.galeus, S. canicula*)	1	1	1	0	0	0	1
(*C. ventriosum*)	?	1	1	0	0	0	1
Squatiniformes (*S. californica*)	0	1	1	1	1	1	0
Squaliformes (*E. spinax, C. crepidater*)	1	1	1	0	0	0	0
(*S. acanthias*)	?	1	1	1	1	1	?
Hexanchiformes (*N. cepedianus*)	?	1	?	0	?	0	?
Chimaeriformes (*H. colliei, C. monstrosa*)	1	1	1	0	0	0	0
(*C. millii*)	?	1	0	0	0	0	?

Ancestral character
Derived character